

## Binding energies of excited shallow acceptor states in GaAs/Ga<sub>1-x</sub>Al<sub>x</sub>As quantum wells

Alfredo Pasquarello and Lucio Claudio Andreani\*

*Institut de Physique Théorique, Ecole Polytechnique Fédérale de Lausanne,  
PHB-Ecublens, CH-1015 Lausanne, Switzerland  
and Scuola Normale Superiore, I-56100 Pisa, Italy*

Ryszard Buczko

*Institute of Physics, Polish Academy of Sciences, PL-02-668 Warsaw, Poland  
and Scuola Normale Superiore, I-56100 Pisa, Italy*

(Received 5 May 1989)

Binding energies of shallow acceptor states in GaAs/Ga<sub>1-x</sub>Al<sub>x</sub>As quantum wells are calculated as a function of the well width. The complex valence-band structure is taken into account in a four-band effective-mass theory. The acceptor envelope function is expanded in valence envelope functions in the two-dimensional  $\mathbf{k}$  space. In this way, the boundary conditions are satisfied by construction. The effect of different dielectric constants in well and barrier materials is taken into account by considering infinite series of image charges. This method of calculation is appropriate for all positions of the acceptor centers, both inside the well and in the barrier, and is particularly suited to evaluate binding energies of excited states. Examples of charge-density distributions of ground and excited states are presented for different positions of the acceptor centers. A first-order perturbation calculation is used to obtain the binding energy of the ground state for on-center acceptors. Theoretical predictions of the transition energies from ground to excited states are found to be in good agreement with available experimental data obtained from far-infrared absorption measurements.

### I. INTRODUCTION

Owing to continuous developments and improvements of crystal-growth techniques, such as molecular-beam epitaxy (MBE),<sup>1</sup> nowadays it is possible to obtain high-quality heterostructures composed of alternating semiconductor layers. Because of the possibility of varying within large bounds the width, the composition, and the doping concentration of the layers, the study of such structures has attracted considerable interest from an experimental as well as from a theoretical point of view. Moreover, the possibility of varying artificially the physical properties is a major advantage for applications in electronic devices. The width of the layers can be varied from several angstroms to several hundred angstroms and can be controlled on an atomic scale, yielding abrupt interfaces between different semiconductors. The background-impurity concentration is low, and intrinsic phenomena dominate the luminescence spectra;<sup>2</sup> extrinsic properties, attributed to the carbon acceptor, have, however, been observed in nominally undoped samples.<sup>3-5</sup> Further development of the growth techniques have allowed intentional and selective doping:<sup>6-12</sup> it is therefore possible to study how the extrinsic properties vary when the doping profile in the layers is changed.

The most widely studied heterostructure is the GaAs/Ga<sub>1-x</sub>Al<sub>x</sub>As superlattice. In this system the band gap, which increases with the aluminum concentration  $x$ , changes from one layer to another. The electrons in the conduction band as well as the holes in the valence band are mainly confined in the GaAs layers, because the

band-gap discontinuity is distributed between the conduction band (65%) and the valence band (35%). When the barriers are sufficiently thick that coupling between different wells can be neglected, one deals with a single quantum well. This is the case studied in this paper. We adopt the effective-mass approach, which has successfully been applied to this system,<sup>13-18</sup> the effect of the band-gap discontinuity being taken into account by introducing square-well potentials for the electrons as well as for the holes. This approach gives a quantitative explanation of intrinsic properties, such as binding energies and oscillator strengths of excitons.<sup>19-23</sup>

Extrinsic properties, such as hole-donor, electron-acceptor, donor-acceptor, and acceptor- and donor-bound exciton transitions, have recently attracted more attention.<sup>3-12</sup> The extrinsic properties strongly depend on the position of the impurity inside the well. The finite width of the doping profiles and the fluctuations of the quantum-well width, especially in the case of narrow wells, broaden the features associated with the observed transitions. In order to measure signals due to transitions related to impurities, higher doping concentrations are needed in the quantum well with respect to the bulk. The interaction which occurs between the impurity centers is another major cause of broadening. In spite of these difficulties, not only have features associated with impurity ground states been observed,<sup>3,6,12</sup> but also transitions involving excited impurity states.<sup>5,7-10</sup>

The envelope-function approach, used in the bulk to calculate energy levels of shallow impurities,<sup>24-26</sup> can be extended to quantum-well systems. For the case of

donors, whose energy levels are near the conduction band, the effective-mass Hamiltonian is that of a Coulomb point charge in a square-well potential. Bastard<sup>27</sup> has calculated binding energies assuming infinitely high barriers. Subsequently, others<sup>28-30</sup> have performed more realistic calculations allowing the wave function to penetrate into the barriers. In this case, since effective masses in well and barrier materials are different, appropriate boundary conditions must be used to match the envelope functions at the interfaces.<sup>15</sup>

The problem of calculating the energy levels of a shallow acceptor is more complicated than for the case of a donor, for two main reasons. First, the uppermost valence band is fourfold degenerate at the  $\Gamma$  point, giving rise to heavy- and light-hole levels. In a quantum well, these levels mix at finite values of the in-plane vector  $\mathbf{k}$ : this mixing occurs at a scale of wave vectors of the order of the reciprocal of the acceptor radius,<sup>17,18</sup> and hence the effect of valence-band mixing must be taken into account. Second, since the acceptor binding energy is larger than the separation between subbands at  $\mathbf{k}=\mathbf{0}$ , an accurate representation of acceptor states must include Coulomb coupling between different subbands.

The effective Bohr radius of the acceptor ground state ( $\approx 20$  Å) is much smaller than the effective donor radius, because the heavy-hole mass is much larger than the conduction-band effective mass. Central-cell effects can therefore significantly influence the binding energy of the ground state. In a quantum well, we expect these effects to increase because of confinement.

Masselink *et al.*<sup>31</sup> have calculated *s*-type acceptor states taking the complex valence-band structure into account. The authors have used a basis in  $\mathbf{r}$  space limited to *s* and *d* anisotropic Gaussian functions. Central-cell effects are accounted for by adding an extremely localized potential.

In this paper we present a variational calculation of the binding energies of shallow acceptor states in the effective-mass approximation, based on the quantum-well band structure. The method is analogous to approaches used for the determination of exciton binding energies through an expansion in  $\mathbf{k}$  space of the wave function.<sup>22</sup> We have taken into account the complex valence-band structure in the axial approximation, which neglects non-axial cubic terms. The effect of different band parameters and dielectric constants in the two materials has been included, respectively, by considering appropriate four-component boundary conditions<sup>18</sup> and series of infinite image charges. This method of calculation in  $\mathbf{k}$  space is particularly suited for excited acceptor states, which are extended in  $\mathbf{r}$  space. The binding energies of the  $\Gamma_6$  and  $\Gamma_7$  ground states are less accurately obtained, because of the finite variational expansion set. For large quantum wells, in order to obtain transition energies between ground and excited states, we estimate the shift and the splitting of the ground state by first-order perturbation theory on the bulk impurity states.

The remaining part of this paper is organized as follows. In Sec. II we present the theoretical approach and relate the symmetry properties of the effective-mass Hamiltonian to the symmetry properties of the underlying

ing crystal structure. In Sec. III we present results for binding energies and density distributions of acceptor states for different well widths and impurity positions. In Sec. IV we compare our results to available experimental data. Transition energies are evaluated by estimating the binding energy of the two ground states in first-order perturbation theory. The main conclusions are summarized in Sec. V.

## II. THEORY

We consider a single quantum well, grown in the [001] direction, which we take along the quantization axis  $z$ . The acceptor Hamiltonian is a  $4 \times 4$  matrix operator

$$H = H^{\text{kin}} + H^{\text{qw}} + H^i(z_0), \quad (1)$$

where  $H^{\text{kin}}$  represents the kinetic energy of the holes,  $H^{\text{qw}}$  the confinement potential due to the valence-band discontinuity, and  $H^i(z_0)$  the potential of an impurity center at  $z = z_0$ . The kinetic-energy term  $H^{\text{kin}}$ , quadratic in  $\mathbf{k} = -i\nabla$ , describes the dispersion of the  $\Gamma_8$  valence band, and is given by the Luttinger-Kohn Hamiltonian<sup>32</sup>

$$H^{\text{kin}} = - \begin{pmatrix} P+Q & L & M & 0 \\ L^\dagger & P-Q & 0 & M \\ M^\dagger & 0 & P-Q & -L \\ 0 & M^\dagger & -L^\dagger & P+Q \end{pmatrix}, \quad (2)$$

where

$$P = \frac{\gamma_1 \hbar^2}{2m_0} k^2, \quad (3a)$$

$$Q = \frac{\gamma_2 \hbar^2}{2m_0} (k_x^2 + k_y^2 - 2k_z^2), \quad (3b)$$

$$L = - \frac{i\sqrt{3}\gamma_3 \hbar^2}{m_0} (k_x - ik_y)k_z, \quad (3c)$$

$$M = \frac{\sqrt{3}\hbar^2}{4m_0} (\gamma_2 - \gamma_3)(k_x + ik_y)^2 + \frac{\sqrt{3}\hbar^2}{4m_0} (\gamma_2 + \gamma_3)(k_x - ik_y)^2, \quad (3d)$$

where  $\gamma_1$ ,  $\gamma_2$ , and  $\gamma_3$  are the Luttinger parameters<sup>33</sup> describing the  $\Gamma_8$  valence band. Inside the quantum well ( $|z| \leq L/2$ ) these parameters correspond to those of the well material, and, in the barrier, to those of the barrier material. In Eq. (2) small  $\mathbf{k}$ -linear terms, originating from the lack of inversion symmetry of the zinc-blende lattice, have been neglected.<sup>34</sup>  $H^{\text{qw}}$  is a square-well potential:

$$H^{\text{qw}} = \begin{cases} 0 & \text{for } |z| \leq L/2 \\ -V & \text{for } |z| \geq L/2 \end{cases}, \quad (4a)$$

$$(4b)$$

where  $V$  is the valence-band discontinuity and  $L$  the well width.  $H^i(z_0)$  is the potential of a point charge in a system of three dielectrics separated by two infinite planes. In order to satisfy the Maxwell boundary conditions, the potential must contain an infinite series of image charges. If  $|z_0| \leq L/2$ , the potential for a point charge is

$$H^i(z_0) = \begin{cases} \frac{\xi e^2}{\epsilon'} \sum_{n=0}^{\infty} \frac{(1-\xi)^n}{R(z_n^-)} & \text{for } z \geq L/2, \\ \frac{e^2}{\epsilon} \left[ \frac{1}{R(z_0)} + \sum_{n=1}^{\infty} (1-\xi)^n \left[ \frac{1}{R(z_n^+)} + \frac{1}{R(z_n^-)} \right] \right] & \text{for } |z| \leq L/2, \\ \frac{\xi e^2}{\epsilon'} \sum_{n=0}^{\infty} \frac{(1-\xi)^n}{R(z_n^+)} & \text{for } z \leq -L/2, \end{cases} \quad (5a)$$

$$H^i(z_0) = \begin{cases} \frac{e^2}{\epsilon'} \left[ \frac{1}{R(z_0)} + \frac{\xi-1}{R(L-z_0)} + \xi \xi' \sum_{n=0}^{\infty} \frac{(1-\xi)^{2n+1}}{R(z_{2n+1})} \right] & \text{for } z \geq L/2, \\ \frac{\xi' e^2}{\epsilon} \sum_{n=0}^{\infty} \frac{(1-\xi)^n}{R(z_n)} & \text{for } |z| \leq L/2, \\ \frac{\xi \xi' e^2}{\epsilon'} \sum_{n=0}^{\infty} \frac{(1-\xi)^{2n}}{R(z_{2n})} & \text{for } z \leq -L/2, \end{cases} \quad (6a)$$

$$H^i(z_0) = \begin{cases} \frac{e^2}{\epsilon'} \left[ \frac{1}{R(z_0)} + \frac{\xi-1}{R(L-z_0)} + \xi \xi' \sum_{n=0}^{\infty} \frac{(1-\xi)^{2n+1}}{R(z_{2n+1})} \right] & \text{for } z \geq L/2, \\ \frac{\xi' e^2}{\epsilon} \sum_{n=0}^{\infty} \frac{(1-\xi)^n}{R(z_n)} & \text{for } |z| \leq L/2, \\ \frac{\xi \xi' e^2}{\epsilon'} \sum_{n=0}^{\infty} \frac{(1-\xi)^{2n}}{R(z_{2n})} & \text{for } z \leq -L/2, \end{cases} \quad (6b)$$

$$H^i(z_0) = \begin{cases} \frac{e^2}{\epsilon'} \left[ \frac{1}{R(z_0)} + \frac{\xi-1}{R(L-z_0)} + \xi \xi' \sum_{n=0}^{\infty} \frac{(1-\xi)^{2n+1}}{R(z_{2n+1})} \right] & \text{for } z \geq L/2, \\ \frac{\xi' e^2}{\epsilon} \sum_{n=0}^{\infty} \frac{(1-\xi)^n}{R(z_n)} & \text{for } |z| \leq L/2, \\ \frac{\xi \xi' e^2}{\epsilon'} \sum_{n=0}^{\infty} \frac{(1-\xi)^{2n}}{R(z_{2n})} & \text{for } z \leq -L/2, \end{cases} \quad (6c)$$

where  $\xi' = 2\epsilon/(\epsilon' + \epsilon)$  and  $z_n = (-1)^n(nL + z_0)$ . With our method of solution it is possible to take into account the infinite series of image charges.

The acceptor Hamiltonian  $H$  acts on a four-component envelope function  $\underline{F} = (F^{3/2}, F^{1/2}, F^{-1/2}, F^{-3/2})$ , and the electronic wave function is given by  $\psi(\mathbf{r}) = \sum_s F^s |\frac{3}{2}s\rangle$  where the spin index  $s$  runs over the set  $\{\frac{3}{2}, \frac{1}{2}, -\frac{1}{2}, -\frac{3}{2}\}$  and where  $|\frac{3}{2}s\rangle$  are the  $\Gamma_8$  Bloch functions. At the barriers the envelope function  $\underline{F}$  must satisfy appropriate current-conserving boundary conditions.<sup>17</sup>

We expand the acceptor envelope function  $\underline{F}$  in the basis of valence envelope functions  $v_{nk}^s(z)e^{ik \cdot \rho}$ , which are eigenstates of the Hamiltonian  $H^{\text{kin}} + H^{\text{qw}}$ , not containing the impurity potential. We obtain

$$F^s(\rho, \theta, z) = \sum_n \int d\mathbf{k} G_n(\mathbf{k}) v_{nk}^s(z) e^{ik \cdot \rho}, \quad (7)$$

where  $\rho = (\rho, \theta)$  is the in-plane coordinate and  $\mathbf{k} = (k, \alpha)$  is the Bloch vector of the subbands, which reflects the translational invariance in the  $x$ - $y$  plane.

The valence envelope functions  $v_{nk}^s(z)$  are found by a method of solution which is an extension of the particle-in-a-box problem of quantum mechanics: the effective-mass equation is solved in each bulk material and the solutions are matched with appropriate boundary conditions at the interfaces.<sup>18</sup> This gives simple analytical wave functions for the valence envelope functions. The components of each envelope function turn out to be trigonometric functions inside the well and decreasing exponentials outside.

With the above-described choice of the valence envelope functions, the calculation of all matrix elements of

the impurity potential is considerably simplified. Another major advantage of expansion (7) is that the acceptor envelope function satisfies, by construction, the current-conserving boundary conditions. In this way the effect of the different band parameters in well and barrier materials is taken into account. In expansion (7),  $n$  runs over all the discrete subbands in the quantum well. We suppose that the quantum well is deep enough to neglect the contribution of continuum states. It should be stressed that, in general, an acceptor state *cannot* be referred to a particular subband, i.e., expansion (7) over the subbands  $n$  is essential. This is due to the fact that the binding energy is larger than the separation between subbands, and should be compared with the case of excitons, where the binding energy is much smaller and Coulomb coupling between subbands is a correction.<sup>22</sup> Assigning an acceptor to a particular subband is possible only for highly excited states, which have a much smaller binding energy.

In our calculations we neglect the first term of  $M$  in Eq. (3d), which depends on the difference between  $\gamma_2$  and  $\gamma_3$ : in this way we obtain a Hamiltonian that is invariant under rotations around the  $z$  axis (axial approximation).<sup>17</sup> If we consider the acceptor Hamiltonian of Baldereschi and Lipari,<sup>26</sup> this approximation consists of keeping not only the full spherical Hamiltonian, but also the axially invariant cubic operator  $T_0^4$  defined in Ref. 26. This latter term is effective in first-order perturbation theory and is taken fully into account in our approximation. The neglected terms  $T_{-4}^4$  and  $T_4^4$  are only effective in second-order perturbation theory and their effect is small when the splitting between the quantum-well acceptor states is much greater than the shift due to the cubic contribution to the Hamiltonian.

Because of axial symmetry, the  $z$  component of the total angular momentum is a good quantum number: we denote it  $m$ . Since  $m$ , for each spin component, is the sum of the angular momentum of the envelope function and of the corresponding Bloch function, it follows that the acceptor envelope function has the form

$$F_m^s(\rho, \theta, z) = e^{i(m-s)\theta} f_m^s(\rho, z). \quad (8)$$

It is important to observe that the phase factor  $e^{i(m-s)\theta}$  is different for each spin component: the quantity  $l = m - s$  can be interpreted as an orbital angular momentum for the corresponding spin component of the envelope function. A similar situation occurs for the exciton problem.<sup>19,21,22</sup> We remark that nonaxial terms couple states with  $\Delta m = \pm 4$ , as can be seen from Eq. (2). Because of time-reversal symmetry, for each state with angular momentum  $m$ , there is a degenerate state with an opposite value of  $m$ . We shall call  $m$  angular momentum, because the electronic wave function  $\psi_m = \sum_s F_m^s | \frac{3}{2} s \rangle$  transforms under the rotation symmetry operators of  $T_d$  as a wave function of definite  $z$  component of angular momentum  $m$ .

The angular dependence of the acceptor envelope function can be extracted from Eq. (7) by observing that, in the axial approximation, the valence envelope function has the following dependence on the angle  $\alpha$  of  $\mathbf{k}$ :

$$v_{n(k, \alpha)}^s(z) = e^{-is\alpha} v_{n(k, 0)}^s(z). \quad (9)$$

If we choose  $G_n(\mathbf{k}) = e^{im\alpha} g_n(k)$  and perform the angular integral, we obtain an explicit form for the envelope function with definite angular momentum  $m$ ,

$$F_m^s(\rho, \theta, z) = 2\pi(i)^{m-s} e^{i(m-s)\theta} \times \sum_n \int dk k g_n(k) v_{n(k, 0)}^s(z) J_{m-s}(k\rho), \quad (10)$$

where  $J_{m-s}$  are Bessel functions. Equation (10) shows that a spin component with orbital angular momentum  $l = m - s$  behaves like  $\rho^l$  for small  $\rho$ .

The valence envelope functions  $v_{n(k, 0)}^s(z)$  can be chosen to be real. In the numerical calculations care must be taken to choose the sign in a continuous way when  $k$  is varied. Thus  $g_n(k)$  is a continuous function of  $k$ .

It is important to remark that the subband Hamiltonian  $H^{\text{kin}} + H^{\text{qw}}$  is invariant under specular reflection with respect to the  $x$ - $y$  plane. The reflection operator  $\sigma$  is given, apart from an overall phase, by

$$\sigma F^s(\rho, \theta, z) = (-1)^{s-1/2} F^s(\rho, \theta, -z). \quad (11)$$

The subbands can thus be classified as even (*gerade*) or odd (*ungerade*) with respect to this operator. It has been shown that *gerade* and *ungerade* valence envelope functions are degenerate by time-reversal symmetry.<sup>18</sup> For  $z_0 \neq 0$ ,  $\sigma$  and  $H^i(z_0)$  do not commute and the valence envelope functions with both parities with respect to  $\sigma$  have to be considered in the expansion. The angular momentum  $m$  is still a good quantum number and, by time-reversal symmetry, each eigenstate is degenerate with an

eigenstate of angular momentum  $-m$ . For  $z_0 = 0$  the full Hamiltonian is invariant under specular reflection. Thus in this case also the acceptor states can be classified as *gerade* ( $g$ ) and *ungerade* ( $u$ ) and only the valence envelope functions of the corresponding symmetry need to be considered in expansion (7). By time-reversal symmetry each acceptor state  $[m, u]$  will be degenerate with a state  $[-m, g]$ .

The acceptor states of the matrix operator  $H$ , for  $z_0 = 0$ , also have definite parity (which we shall denote by a plus or a minus sign) under space inversion  $I$ ,

$$IF^s(\mathbf{r}) = F^s(-\mathbf{r}), \quad (12)$$

not to be confused with  $\sigma$ . The inversion  $I$  commutes with the time-reversal operator and therefore each Kramers doublet  $[m, u; -m, g]$  has definite parity under  $I$ .

In order to understand the symmetry of the acceptor envelope eigenfunctions according to the underlying crystal symmetry group, we study the compatibility relations between the representations of the symmetry group of the axially invariant Hamiltonian and those of the actual symmetry group. These relations can be obtained by analyzing the transformation properties of the full electronic wave function. For a  $T_d$  crystal point group, the electronic wave function contains  $\Gamma_8$  valence Bloch functions and transforms according to a representation of  $T_d$ . For  $z_0 = 0$ , because of the quantum well, the symmetry is reduced from bulk  $T_d$  to  $D_{2d}$ ,<sup>35</sup> which allows only two two-dimensional representations  $\Gamma_6$  and  $\Gamma_7$ . If  $z_0 \neq 0$ , the symmetry group reduces to  $C_{2v}$  and all eigenstates trans-

TABLE I. Relation between the symmetry of the eigenstates of the effective-mass Hamiltonian and the symmetry of the electronic states for an impurity in a quantum well built of  $T_d$  and  $O_h$  crystal materials. The case with the impurity at the center of the quantum well ( $z_0 = 0$ ) as well as the off-center case ( $z_0 \neq 0$ ) are considered.

Axial symmetry	Bulk $T_d$	
	$z_0 = 0$	Bulk $O_h$
	$D_{2d}$	$D_{4h}$
$[(\frac{3}{2} + 4k)u, -(\frac{3}{2} + 4k)g]^+$	$\Gamma_6$	$\Gamma_6^+$
$[(\frac{1}{2} + 4k)u, -(\frac{1}{2} + 4k)g]^-$	$\Gamma_6$	$\Gamma_7^-$
$[(-\frac{1}{2} + 4k)u, -(-\frac{1}{2} + 4k)g]^+$	$\Gamma_7$	$\Gamma_7^+$
$[(-\frac{3}{2} + 4k)u, -(-\frac{3}{2} + 4k)g]^-$	$\Gamma_7$	$\Gamma_6^-$
	$z_0 \neq 0$	
	$C_{2v}$	$C_{4v}$
$[(\frac{3}{2} + 4k), -(\frac{3}{2} + 4k)]$	$\Gamma_5$	$\Gamma_6$
$[(\frac{1}{2} + 4k), -(\frac{1}{2} + 4k)]$	$\Gamma_5$	$\Gamma_7$
$k = 0, \pm 1, \pm 2, \dots$		

form like  $\Gamma_5$ . For comparison, we have also analyzed the case of an  $O_h$  crystal symmetry group. The results are summarized in Table I.

We must now solve the eigenvalue equation  $HF = EF$ . Substituting expansion (7) for  $F$  and using the orthonormality relation between valence envelope functions,

$$(2\pi)^2 [E_n(k) - E] g_n(k) + \sum_{n'} \int_0^\infty dk' k' \int_0^{2\pi} d(\Delta\alpha) \langle n\mathbf{k} | H^i(z_0) | n'\mathbf{k}' \rangle e^{-im\Delta\alpha} g_{n'}(k') = 0, \quad (14)$$

where  $E_n(k)$  gives the subband dispersion,  $\Delta\alpha = \alpha - \alpha'$ , and

$$\langle n\mathbf{k} | H^i(z_0) | n'\mathbf{k}' \rangle = \int_{-\infty}^\infty dz \left[ \int d\rho H^i(z_0) e^{i(\mathbf{k}' - \mathbf{k}) \cdot \rho} \right] \sum_s [v_{nk}^s(z)]^* v_{n'k'}^s(z) e^{is\Delta\alpha}. \quad (15)$$

For the case  $H^i(z_0) = e^2 / [\epsilon R(z_0)]$  the integral in the in-plane coordinate can be carried out analytically using<sup>36</sup>

$$\int d\rho \frac{e^{i(\mathbf{k}' - \mathbf{k}) \cdot \rho}}{[\rho^2 + (z - z_0)^2]^{1/2}} = \frac{2\pi}{\Delta k} e^{-|z - z_0| \Delta k}, \quad (16)$$

where  $\Delta k = [k^2 + (k')^2 - 2kk' \cos(\alpha - \alpha')]^{1/2}$ . The valence envelope functions are linear combinations of trigonometric functions.<sup>18</sup> Thus, the  $z$  integral can also be performed analytically. The result depends on  $z_0$  only via exponential factors: hence, the sum over image charges reduces to a geometric series. It is a distinct virtue of the present theory that the matrix elements (15) of the Coulomb potentials are calculated analytically, also including the effect of different band parameters and dielectric constants in well and barrier materials.

Since the integral equation (14) for  $g_n(k)$  is real, as can be seen by analyzing the dependence of expression (15) on

$$H_{nl, n'l'} = \delta_{nn'} \int_0^\infty dk k E_n(k) h_l(k) h_{l'}(k) + \frac{1}{2\pi^2} \int_0^\infty dk k \int_0^\infty dk' k' \int_0^\pi d\Delta\alpha \langle n\mathbf{k} | H^i(z_0) | n'\mathbf{k}' \rangle e^{-im\Delta\alpha} h_l(k) h_{l'}(k') \quad (20)$$

and

$$N_{nl, n'l'} = \delta_{nn'} \int_0^\infty dk k h_l(k) h_{l'}(k). \quad (21)$$

The real eigenvalue problem (19) can be solved by numerical methods that simultaneously diagonalize the matrices  $H$  and  $N$  of Eqs. (20) and (21), yielding the coefficients  $A_{nl}$  as the corresponding eigenvectors. In this way we can find the acceptor ground state as well as the excited states. Different eigenvalue problems are solved for different values of  $m$  (and, for  $z_0 = 0$ , for different parities with respect to  $\sigma$ ). The integrand in the second term of Eq. (20) is singular at  $\mathbf{k} = \mathbf{k}'$ , although the integral itself is finite. The integral is evaluated by adding and subtracting a function that removes the divergence, but which can be integrated analytically. The remaining three-dimensional integral has a smooth dependence on  $k$ ,  $k'$ , and  $\Delta\alpha$ , and is evaluated numerically with the Gaussian method.

$$\sum_s \int d\mathbf{r} [v_{n'\mathbf{k}'}^s(z)]^* v_{n\mathbf{k}}^s(z) e^{i(\mathbf{k} - \mathbf{k}') \cdot \rho} = (2\pi)^2 \delta_{nn'} \delta(\mathbf{k} - \mathbf{k}'), \quad (13)$$

we obtain for an acceptor state of angular momentum  $m$  the following integral equation for  $g_n(k)$ :

$\Delta\alpha$ , we solve (14) by expanding  $g_n(k)$  into nonorthogonal hydrogenic wave functions  $h_l(k)$  of different radii  $1/\alpha_l$ :

$$g_n(k) = \sum_l A_{nl} h_l(k), \quad (17)$$

where

$$h_l(k) = \frac{\alpha_l}{(\alpha_l^2 + k^2)^{3/2}}. \quad (18)$$

The  $A_{nl}$  are real variational parameters, while the  $\alpha_l$  are chosen to cover the relevant physical range. We finally obtain a generalized eigenvalue problem for the coefficients  $A_{nl}$ ,

$$\sum_{n'l'} H_{nl, n'l'} A_{n'l'} = E \sum_{n'l'} N_{nl, n'l'} A_{n'l'}, \quad (19)$$

where

### III. RESULTS

We consider GaAs/Ga<sub>1-x</sub>Al<sub>x</sub>As quantum wells with varying well width  $L$ . In numerical calculations, the dielectric constants and Luttinger parameters are taken to be<sup>37</sup>

$$\epsilon = 12.56, \quad \gamma_1 = 6.85, \quad \gamma_2 = 2.10, \quad \gamma_3 = 2.90$$

for GaAs, and

$$\epsilon' = 9.80, \quad \gamma_1 = 3.45, \quad \gamma_2 = 0.68, \quad \gamma_3 = 1.29$$

for AlAs. Parameters for Ga<sub>1-x</sub>Al<sub>x</sub>As are obtained by linear interpolation. The band-gap difference is given by  $\Delta E_g = 1247 \times x$  meV,<sup>38</sup> and we assume an offset ratio of  $\Delta E_v / \Delta E_g = 0.35$ , so that  $V = 0.35 \times 1247 \times x$  meV.

In Fig. 1 we present, for an impurity located at  $z_0 = 0$ , the energy levels for the ground and first-excited states for aluminum concentration  $x = 0.4$ . The well width ranges from 25 to 200 Å. We have used a shorthand notation identifying  $[mu, -mg]^\pm$  by  $|m|(\pm)$ . The acceptor

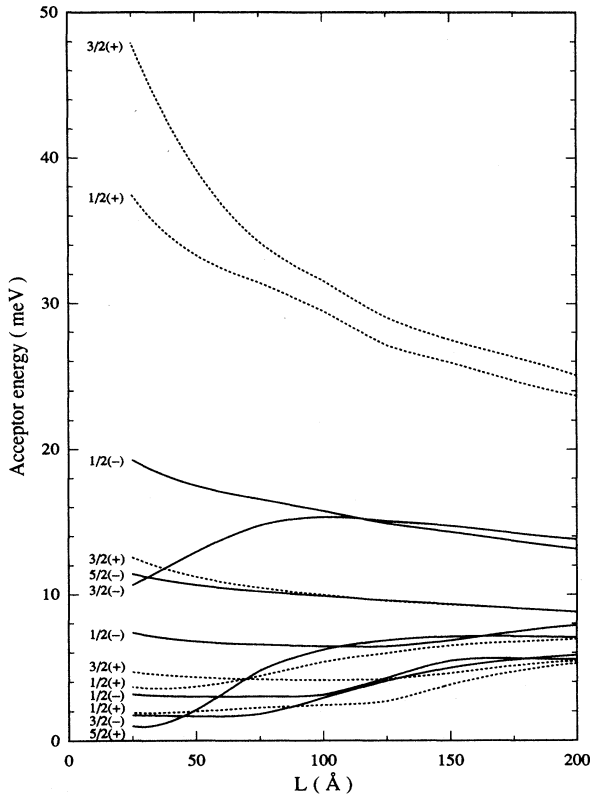


FIG. 1. Energy levels for on-center acceptors in GaAs/Ga<sub>0.6</sub>Al<sub>0.4</sub>As quantum wells as a function of the well width. Acceptor energies are given as binding energies with respect to the first heavy-hole subband. The dashed curves represent the acceptor energy for states with the symmetry of the two ground states. The solid lines correspond to states of different symmetry and are more accurate. The absolute value of the angular momentum  $m$  and the parity with respect to inversion indicate the symmetry of the acceptor states.

energy levels are given as binding energies with respect to the first heavy-hole subband (HH1). From Fig. 1 we notice that, for some excited states, the energies with respect to HH1 decrease with decreasing well width. This effect can be understood because these excited states can mainly be associated with higher subbands, whose energy separation with HH1 increases with decreasing well width.

The number of subbands we keep in expansion (7) depends on the width of the quantum well and on the height of the barriers. We always retain all the bound subbands. We notice that not all the subbands, which are bound at  $k=0$ , can be taken into account, as some of them enter the continuum at a finite  $k$  value.<sup>18</sup> The fact that the number of basis subbands is different for different well widths is the reason for some bumps in Fig. 1. The neglect of the subband continuum greatly affects the binding energies of the two  $[\frac{3}{2}u, -\frac{3}{2}g]^+$  ( $\Gamma_6$ ) and  $[-\frac{1}{2}u, \frac{1}{2}g]^+$  ( $\Gamma_7$ ) ground states, which are underestimated by about 6 meV at 200 Å. The binding energies of higher excited states of different symmetry are, however,

much more accurately calculated. By studying convergence as a function of the energy region covered by the bound subbands in a large quantum well, we estimate that the residual error for these excited states be less than a few tenths of a meV.

The reason for the different influences of the subband continuum on ground and excited states can be understood by considering the value of the binding energy. In the limit of wide wells, the binding energy of the ground state is about 30 meV, while the binding energies of the excited states are about 15 meV or less. Large binding energies correspond to small typical radii and, therefore, a larger region of the Brillouin zone is needed to describe the wave function. The  $z$  quantization of the subbands is the quantum-well analog of the bulk dispersion as a function of  $k_z$ . Thus, when the needed  $k$  region increases, more subbands must be taken into account. In order to reach convergence also for the binding energies of the ground states, we should include quantum-well wave functions of the continuum in our variational set. This could be done by discretizing the continuum in a large box: the method, however, would become computationally cumbersome.

We remark that the binding energies of the excited states with the same symmetry of the ground states are less accurate than the other excited states, because the orthogonality condition relates them to an unsatisfactory ground state. In the axial approximation the excited states of different symmetries are obtained by a separate calculation and are not influenced by the accuracy in the determination of the ground state. In fact, binding energies of excited states are obtained with an accuracy similar to that of the exciton calculation,<sup>22</sup> as can be expected from the fact that exciton binding energies are of the same order of magnitude. As this method does not provide accurate results for the ground states, we have not considered central-cell effects, nor effects of spatially dependent screening.<sup>39</sup>

The effect of the dielectric mismatch is essentially given by the expectation value of the potential of the first image charges on the acceptor wave function.<sup>40</sup> This effect increases the binding energy, since, for  $\epsilon' < \epsilon$ , the first image charges have the same sign as the impurity charge. The correction to the binding energy of the first excited state is about 10% for a well width of 50 Å and decreases to about 4% for a well of 150 Å. The effect does not change significantly when the impurity position is shifted towards the barriers, as the charge density of the wave function remains mainly inside the well.

In order to check the validity of the axial approximation, we have performed a calculation of the bulk acceptor levels with an axially invariant Hamiltonian and with the complete cubic Hamiltonian. The bulk acceptor Hamiltonian has been solved as described in Ref. 41. In Table II we present the results. For comparison, we have included the results obtained with the spherical Hamiltonian of Baldereschi and Lipari.<sup>26</sup> From Table II we deduce that the axial approximation accounts for most of the cubic effect. In the quantum well this approximation should work even better, as states of different  $z$  component of angular momentum are not only split by cubic

TABLE II. Binding energies of ground and excited states for the GaAs bulk acceptor Hamiltonian in the spherical approximation, in the axial approximation, and with the full cubic contribution. We have used  $\gamma_1=6.85$ ,  $\gamma_2=2.10$ ,  $\gamma_3=2.90$ , and  $\epsilon=12.53$ .

Spherical approx.		Axial approx.		Cubic Hamiltonian	
Symmetry	$E$ (meV)	Symmetry	$E$ (meV)	Symmetry	$E$ (meV)
$1S_{3/2}$	27.43	$[\frac{3}{2}u, -\frac{3}{2}g]^+$	28.41	$\Gamma_8$	28.94
		$[-\frac{1}{2}u, \frac{1}{2}g]^+$	28.22		
$2P_{3/2}$	11.76	$[-\frac{3}{2}u, \frac{3}{2}g]^-$	12.44	$\Gamma_8$	12.77
		$[\frac{1}{2}u, -\frac{1}{2}g]^-$	12.29		
$2S_{3/2}$	8.13	$[\frac{3}{2}u, -\frac{3}{2}g]^+$	8.51	$\Gamma_8$	8.70
		$[-\frac{1}{2}u, \frac{1}{2}g]^+$	8.44		
$2P_{5/2}$	6.89	$[\frac{1}{2}u, -\frac{1}{2}g]^-$	7.82	$\Gamma_8$	8.01
		$[\frac{5}{2}u, -\frac{5}{2}g]^-$	7.51		
		$[-\frac{3}{2}u, \frac{3}{2}g]^-$	6.06		
$3P_{3/2}$	5.31	$[-\frac{3}{2}u, \frac{3}{2}g]^-$	5.69	$\Gamma_8$	5.86
		$[\frac{1}{2}u, -\frac{1}{2}g]^-$	5.60		
$3D_{5/2}$	5.14	$[-\frac{1}{2}u, \frac{1}{2}g]^+$	5.74	$\Gamma_8$	5.93
		$[-\frac{5}{2}u, \frac{5}{2}g]^+$	5.58		
		$[\frac{3}{2}u, -\frac{3}{2}g]^+$	4.75		

terms, but also by the barrier potential. Table II shows that the axial approximation remains valid even in the large-well limit, when the effect of the barrier potential is negligible. In particular, in the case of the spherical  $2P_{5/2}$  state, it is interesting to notice how the axial approximation reproduces the splitting between the  $\Gamma_8$  and  $\Gamma_7$  states of the full cubic Hamiltonian, whereas these states turn out to be degenerate in the spherical approximation.

We plot in Fig. 2 the binding energies of the ground and excited states for on-edge acceptors ( $z_0=L/2$ ) as a function of the well width  $L$ . Now the states are classified only by the  $z$  component of angular momentum  $m$ . Since the binding energies are smaller compared to those of the on-center case, our method is expected here to give more accurate results also for the ground states.

We present in Fig. 3 the acceptor spectrum as a function of the impurity position along the  $z$  axis for a 100-Å GaAs/Ga<sub>0.6</sub>Al<sub>0.4</sub>As quantum well. The binding energies reach a maximum for on-center acceptors, and decrease as the acceptor is moved away from the well center. At  $z_0=100$  Å, well inside the barrier, the binding energy of the ground state is still about 8 meV. The density of acceptors with a given binding energy is proportional to the reciprocal of the slope of the binding energy with respect to the position,<sup>27</sup> and is important because of the finite width of the acceptor doping profile. From Fig. 3 we see that, in the case of a uniformly doped (100 Å/100 Å) superlattice, most acceptors have binding energies which are near those for an on-center acceptor or those obtained for an acceptor at the center of the barrier. For the parameters of Fig. 3, there is no peak in the density of states due to on-edge acceptors.

In Fig. 3 the curves which correspond to states with

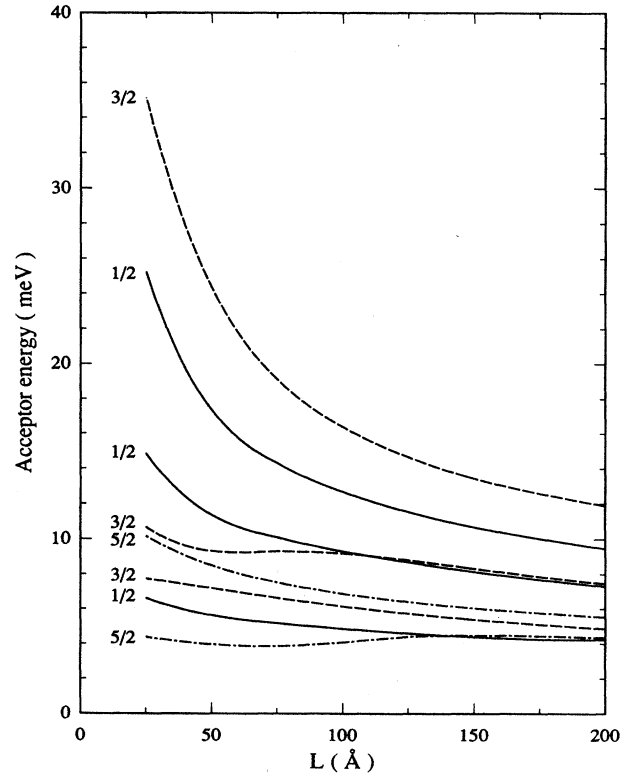


FIG. 2. Energy levels for on-edge acceptors in GaAs/Ga<sub>0.6</sub>Al<sub>0.4</sub>As quantum wells as a function of the well width. Acceptor energies are given as binding energies with respect to the first heavy-hole subband. The symmetry of the acceptor states is indicated by the absolute value of  $m$ .

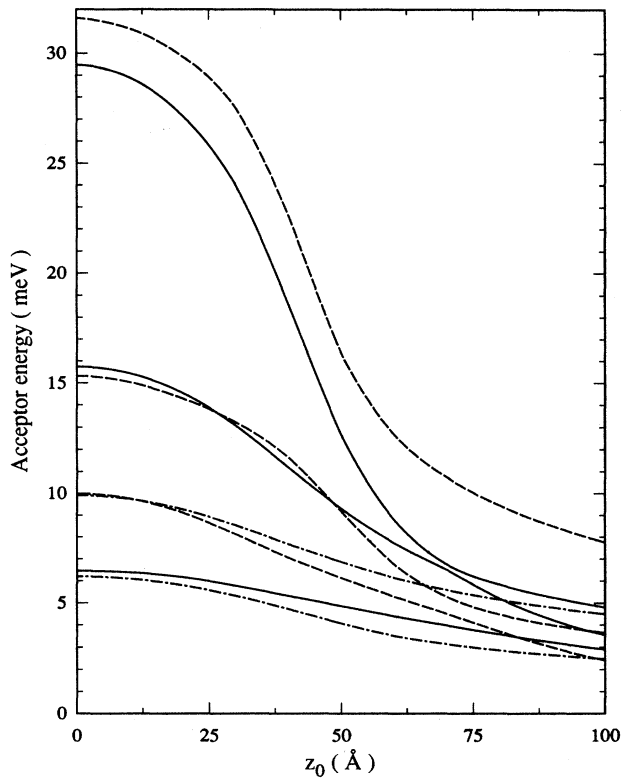


FIG. 3. Energy levels as a function of the acceptor position in a 100-Å GaAs/Ga<sub>0.6</sub>Al<sub>0.4</sub>As quantum well. Solid lines indicate the acceptor energies of states with  $m = \frac{1}{2}$ , dashed lines with  $m = \frac{3}{2}$ , and dotted-dashed lines with  $m = \frac{5}{2}$ .

the same symmetry do not cross. At  $z_0 \approx 70$  Å, the  $m = \frac{1}{2}$  ground and first-excited states, as well as the  $m = \frac{3}{2}$  first- and second-excited states, anticross.

In Fig. 4 we present the charge-density profile along the  $z$  axis of the lowest acceptor states for a 100-Å GaAs/Ga<sub>0.6</sub>Al<sub>0.4</sub>As quantum well. We consider (a) on-center acceptors ( $z_0 = 0$ ), (b) on-edge acceptors ( $z_0 = 50$  Å), and (c) acceptors inside the barrier at  $z_0 = 100$  Å. Because of the axial approximation, only states with  $m = \frac{1}{2}$  or  $\frac{3}{2}$  have finite density on the  $z$  axis [see Eq. (10)]. As the acceptor moves away from the well center, the density along the  $z$  axis decreases, because the acceptor states become more extended.

In Fig. 4(a), the first-excited state is of different parity with respect to inversion and its wave function has a node at the center of the well. For on-edge acceptors [Fig. 4(b)] the charge density moves towards the well edge, but is still mainly confined to the quantum well. Although the charge distribution is now asymmetric, the wave functions have essentially kept their  $s$  or  $p$  character. In Fig. 4(c) we see that when the acceptor moves far into the barrier, the charge distribution is still mainly confined to the well. Moreover, it moves back to the well center and is less asymmetric. This effect can be understood because now only the tail of the Coulomb potential is effective, and the confining barriers of the quantum well prevail.

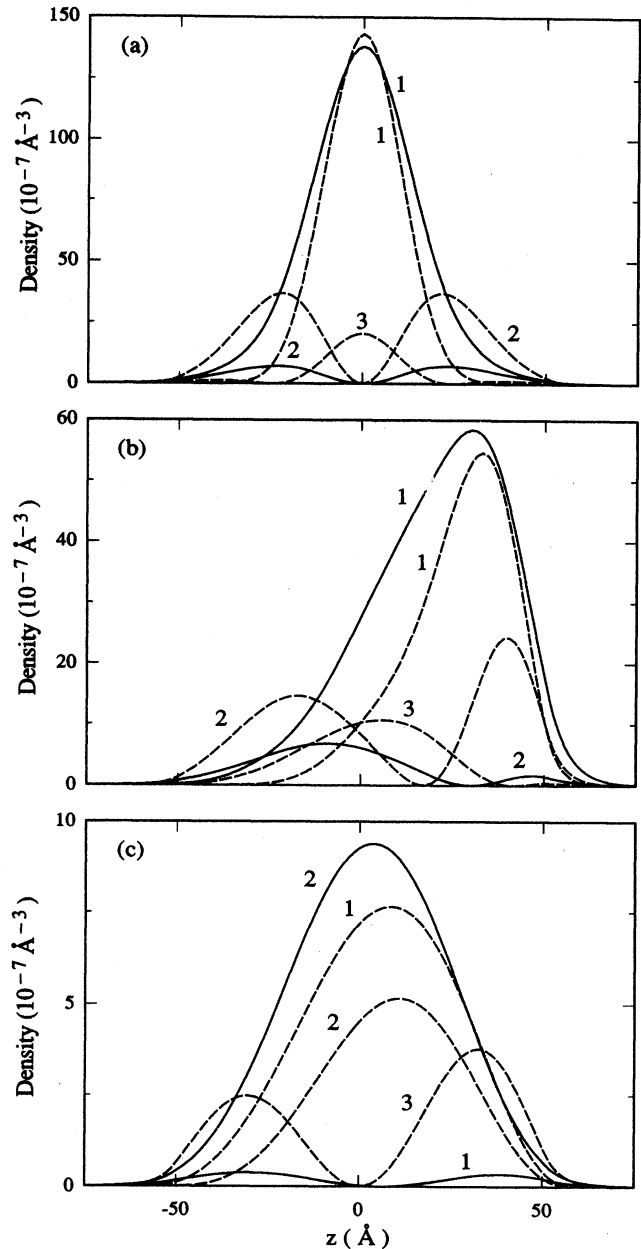


FIG. 4. The charge density along the  $z$  axis of the first acceptor states in a 100-Å GaAs/Ga<sub>0.6</sub>Al<sub>0.4</sub>As quantum well is plotted for (a) an on-center acceptor ( $z_0 = 0$ ), (b) an on-edge acceptor ( $z_0 = 50$  Å), and for (c) an acceptor at  $z_0 = 100$  Å. Solid lines: states with  $m = \frac{1}{2}$ . Dashed lines: states with  $m = \frac{3}{2}$ . Curves related to states of the same symmetry are numbered following decreasing binding energies.

In the barriers, Coulomb-type states exist at energies above the top of the Ga<sub>1-x</sub>Al<sub>x</sub>As valence band. These states are at much higher energies with respect to the energies we are considering and are degenerate with high-energy quantum-well states.<sup>27</sup> If we compare the curves of Figs. 4(c) and 4(b), we notice that the character of the first two  $m = \frac{1}{2}$  states and of the second and third  $m = \frac{3}{2}$

states are exchanged. This effect illustrates the anticrossings, which had been noted in Fig. 3.

We have also calculated the binding energies for quantum wells with an aluminum concentration  $x=0.3$ , for on-center as well as for on-edge acceptors. For the excited states the binding energies differ from those with  $x=0.4$  by less than the estimated numerical error.

Masselink *et al.*<sup>31</sup> have calculated acceptor binding energies by expanding the wave function in  $r$  space. These authors only calculated binding energies of  $s$ -type states, which correspond to the states with the symmetry of the two ground states. In the large-well limit the method of Masselink *et al.* yields binding energies which are higher than ours and which correctly reproduce the bulk limit. However, when the width of the quantum well is smaller than  $\approx 50$  Å, their results for the ground states are lower than ours. Since our variational results represent a lower bound for the binding energy, the neglect of the subband continuum in the expansion set cannot explain the discrepancy. The reason for the discrepancy might be due to the fact that their expansion is limited to symmetry-adapted  $s$  and  $d$  orbitals, which in the bulk limit describe the wave function accurately, but which could be insufficient in the case of narrow wells, when the symmetry is strongly altered. Another possible explanation lies in the approximate method used in Ref. 31 to take into account the effect of different band parameters and dielectric constants in well and barrier materials.

Both these effects are even more important for excited states, which are more extended in  $r$  space and "feel" the barrier potential also at larger well widths. We find that the binding energy of the heavy-hole  $2s$  state  $[\frac{3}{2}u, -\frac{3}{2}g]^+$  ( $\Gamma_6$ ) increases for decreasing well width, whereas Masselink *et al.*<sup>31</sup> find an opposite trend; the same is true for the binding energy of the light-hole  $2s$  state  $[-\frac{1}{2}u, \frac{1}{2}g]^+$  ( $\Gamma_7$ ) with respect to the first light-hole subband.

#### IV. TRANSITION ENERGIES BETWEEN GROUND AND EXCITED ACCEPTOR STATES

In order to compare our theoretical results with infrared absorption experiments, it is useful to analyze the selection rules first. If the polarization of the electromagnetic radiation is parallel to the quantization axis, transitions are allowed between states of different  $T_d$  symmetry:  $\Gamma_6 \rightarrow \Gamma_7$  or  $\Gamma_7 \rightarrow \Gamma_6$ . In the case of in-plane polarization, all transitions are allowed. The same selection rules are found for a bulk  $T_d$  crystal with an applied uniaxial stress along a  $\langle 100 \rangle$  direction.<sup>42</sup> It is, however, useful to consider the allowed transitions between eigenstates of the axially invariant effective-mass Hamiltonian, as these generally have a greater oscillator strength. Now,  $z$  polarization does not change the  $z$  component of the angular momentum  $m$ , and allows transitions between states with opposite parity under reflection  $\sigma$  and inversion  $I$ . In the case of  $xy$  polarization, transitions are allowed between states with angular momenta differing by  $\pm 1$ , of the same parity with respect to  $\sigma$ , but of opposite parity with respect to  $I$ .

Reeder *et al.*<sup>8</sup> have performed a far-infrared absorption experiment on Be center-doped quantum wells at a

temperature of 4.2 K. In order to understand the observed transitions, it is important to know the splitting of the ground state as compared to  $k_B T \approx 0.36$  meV. Moreover, to estimate transition energies from ground to excited states, we also need the binding energies of the ground states, which are not accurate enough in our calculation. For large quantum wells, the shift and the splitting of the ground state can be evaluated treating the confinement potential in first-order perturbation theory, as the effective Bohr radius of the ground state is about 20 Å. The wave functions of the fourfold-degenerate  $1S_{3/2}$  ground state are calculated in the spherical approximation, taking into account  $l=0$  as well as  $l=2$  angular orbitals. If  $f_l(r)$  and  $f_h(r)$  are the radial asymptotic functions as defined in Ref. 43, the average shift  $S$  and the splitting  $\Delta$  are found to be

$$S = -V \int_{L/2}^{\infty} r^2 [f_h^2(r) + f_l^2(r)] (1 - L/2r) dr, \quad (22)$$

$$\Delta = V \int_{L/2}^{\infty} r^2 [f_h^2(r) - f_l^2(r)] (L/2r) [1 - (L/2r)^2] dr,$$

where  $V$  is the barrier height as defined in (4). For the acceptor binding energy in the bulk, we use the value of 28.5 meV as measured by Reeder *et al.*<sup>8</sup> The binding energies are found by considering the energy position of the first heavy-hole subband. We notice that the barrier potential  $H^{qw}$  shifts the acceptor levels, as well as the subbands, in the same direction. The shift of the acceptor ground states is, however, much smaller since the wave function is localized. The results obtained for the binding energy are given in Fig. 5. The limit of validity of the perturbation result is reached when the binding energy no longer increases for decreasing well width. We notice that this limit is reached at larger well widths for the light-hole ground state than for the heavy-hole ground state, because the former is more extended in the  $z$  direction.

In Table III we compare our theoretical results for the transition energies from the ground state to excited states

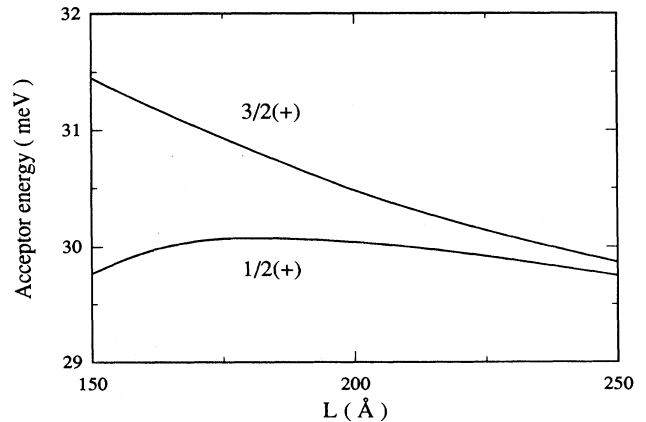


FIG. 5. Acceptor energies of the ground states with respect to the first heavy-hole subband. The shifts with respect to the bulk level of 28.5 meV (Ref. 8) are calculated in first-order perturbation theory in the spherical approximation.

TABLE III. Calculated transition energies from the heavy-hole  $[\frac{3}{2}u, -\frac{3}{2}g]^+$  ground state (indicated by  $g_h$ ) and from the light-hole  $[-\frac{1}{2}u, \frac{1}{2}g]^+$  ground state (indicated by  $g_l$ ) are compared for two quantum-well widths with the data from the absorption experiment of Reeder *et al.* (Ref. 8). We have taken an aluminum concentration of  $x=0.3$ . The reported transitions are allowed for  $xy$  polarization in the axial approximation. The excited states are numbered following decreasing binding energies. Transition energies are in meV.

Transition	150 Å		200 Å	
	Theor.	Expt.	Theor.	Expt.
$g_l \rightarrow 1[-\frac{3}{2}u, \frac{3}{2}g]^-$			16.4	
$g_l \rightarrow 1[\frac{1}{2}u, -\frac{1}{2}g]^-$			17.1	
$g_h \rightarrow 1[\frac{1}{2}u, -\frac{1}{2}g]^-$	17.3	18.6	17.5	17.4
$g_h \rightarrow 1[\frac{5}{2}u, -\frac{5}{2}g]^-$	22.3	24.5	21.8	22.3
$g_h \rightarrow 2[\frac{1}{2}u, -\frac{1}{2}g]^-$	24.7		22.7	
$g_l \rightarrow 2[\frac{1}{2}u, -\frac{1}{2}g]^-$			22.3	
$g_l \rightarrow 2[-\frac{3}{2}u, \frac{3}{2}g]^-$			24.3	
$g_l \rightarrow 3[\frac{1}{2}u, -\frac{1}{2}g]^-$			24.6	
$g_h \rightarrow 3[\frac{1}{2}u, -\frac{1}{2}g]^-$	26.0	26.2	25.0	24.2

with experimental data obtained by Reeder *et al.*<sup>8</sup> In this experiment the electromagnetic radiation is polarized in the layer plane. We have not made a comparison with the data relative to the 100-Å sample because the first-order perturbation result is not accurate for such a small well width. For a quantum well of 150 Å the splitting of the ground state is much larger than  $k_B T$ , and we assume that the observed absorption peaks are due to transitions from the populated ground state to higher excited states. The energies at which the absorption peaks occur should therefore be compared with theoretical results that correspond to allowed transitions from the  $[\frac{3}{2}u, -\frac{3}{2}g]^+$  ground state. For a quantum well of 200 Å the splitting between the two lowest states is about 0.5 meV, which is only slightly larger than  $k_B T$ . In Table III, for this well width, we have also considered the transitions from the  $[-\frac{1}{2}u, \frac{1}{2}g]^+$  ground state, although the corresponding absorption peaks should be weaker.

Starting from the ground state of  $[\frac{3}{2}u, -\frac{3}{2}g]^+$  symmetry, for  $xy$  polarization, the axial approximation allows only transitions to states with  $[\frac{1}{2}u, -\frac{1}{2}g]^-$  or  $[\frac{5}{2}u, -\frac{5}{2}g]^-$  symmetry. Because of the cubic symmetry, transitions to states with other symmetries, such as  $[-\frac{3}{2}u, \frac{3}{2}g]^-$ , are also allowed, but the associated strength is expected to be much smaller.

The lowest absorption peak corresponds to the transition to the first  $[\frac{1}{2}u, -\frac{1}{2}g]^-$  state. In the bulk limit this state is degenerate with the first  $[-\frac{3}{2}u, \frac{3}{2}g]^-$  state and forms the bulk  $2P_{3/2}[\Gamma_8]$  state. In the bulk this transition is identified as the  $G$  line.<sup>44</sup> For this transition we found decreasing transition energies for increasing well width. The decrease is smaller than the estimated numerical error. We believe it is due to the finite variational set, which is based on the bound subbands, and which, therefore, depends on the well width. The transition

from the light-hole ground state to the first  $[-\frac{3}{2}u, \frac{3}{2}g]^-$  state should be observable if both ground states were populated.

The second observed peak is broad and corresponds to transitions to the first  $[\frac{5}{2}u, -\frac{5}{2}g]^-$  state and to the second  $[\frac{1}{2}u, -\frac{1}{2}g]^-$  state. In the bulk limit these states go over into the  $2P_{5/2}[\Gamma_8]$ , and the relative transition corresponds to the  $D$  line. The third transition observed in the absorption experiment can be interpreted as the transition to the third  $[\frac{1}{2}u, -\frac{1}{2}g]^-$  state.

The second  $[-\frac{3}{2}u, \frac{3}{2}g]^-$  state corresponds to the bulk  $2P_{5/2}[\Gamma_7]$  state. In the bulk the main contribution to the  $C$  line comes from the corresponding transition from the ground state, but, in the quantum well, the transitions from the heavy-hole ground state to states with  $[-\frac{3}{2}u, \frac{3}{2}g]^-$  symmetry are forbidden in the axial approximation. The transition from the light-hole ground state to the second  $[-\frac{3}{2}u, \frac{3}{2}g]^-$  state, which, in fact, corresponds to the bulk  $C$  line, is allowed and should be observable at higher temperatures, when the light-hole ground state is more populated.

In conclusion, all observed peaks can be understood as transitions from the heavy-hole ground state. In this interpretation our calculated transition energies agree within 1.5 meV with the experimental data.

## V. CONCLUSIONS

We have calculated binding energies of excited shallow acceptor states in GaAs/Ga<sub>1-x</sub>Al<sub>x</sub>As quantum wells. The valence-band structure has been taken into account by adopting a four-band effective-mass theory. The acceptor envelope function has been expanded into a basis of valence envelope functions of the bound quantum-well subbands. This method is particularly suited to find binding energies of excited states; it is less accurate for the acceptor ground state, which is more sensitive to the subband continuum. The acceptor envelope functions satisfy current-conserving boundary conditions by construction. The effect of different dielectric constants in the two materials has been taken into account by considering infinite series of image charges. Calculations have been performed in the axial approximation, which only neglects small nonaxial cubic terms in the Hamiltonian.

We have presented energy spectra of acceptor excited states as a function of the impurity position. Acceptor positions inside as well as outside the quantum well have been considered. We have shown that, when the impurity moves into the barrier, the charge-density distribution associated to an acceptor state remains mainly located inside the well and its center moves back to the well center as the impurity is moved further in the barrier.

Finally, calculated transition energies have been compared with results from far-infrared absorption experiments. By considering the bulk limit and by comparing the energies of the corresponding allowed transitions as the well width decreases, we have interpreted the acceptor absorption spectrum in GaAs/Ga<sub>1-x</sub>Al<sub>x</sub>As quantum wells.

## ACKNOWLEDGMENTS

We acknowledge fruitful and stimulating discussions with A. Baldereschi, F. Bassani, N. Binggeli, S. Fraizzoli, and A. Quattropani. We are particularly grateful to S. Fraizzoli for allowing us to compare our acceptor binding energies with his unpublished results and to F. Bas-

sani for a critical reading of the manuscript. This work was supported in part by the Italian Consiglio Nazionale delle Ricerche and the Polish Academy of Sciences, in the framework of an exchange agreement. One of the authors (R.B.) acknowledges support from the Scientific Research Program CPBP-01-04 by the Polish Ministry of Science, Higher Education and Technology.

\*Present address: Institut Romand de Recherche Numérique en Physique des Matériaux, PHB-Ecublens, CH-1015 Lausanne, Switzerland.

- <sup>1</sup>See, for example, B. A. Joyce, *Rep. Prog. Phys.* **48**, 1637 (1985).  
<sup>2</sup>R. Dingle, A. C. Gossard, and W. Wiegmann, *Phys. Rev. Lett.* **34**, 1327 (1975); R. C. Miller and D. A. Kleinman, *J. Lumin.* **30**, 520 (1985).  
<sup>3</sup>R. C. Miller, A. C. Gossard, W. T. Tsang, and O. Munteanu, *Phys. Rev. B* **25**, 3871 (1982).  
<sup>4</sup>D. C. Reynolds, K. K. Bajaj, C. W. Litton, P. W. Yu, W. T. Masselink, R. Fisher, and H. Morkoç, *Phys. Rev. B* **29**, 7038 (1984).  
<sup>5</sup>K. T. Tsen, J. Klem, and H. Morkoç, *Solid State Commun.* **59**, 537 (1986).  
<sup>6</sup>R. C. Miller, A. C. Gossard, W. T. Tsang, and O. Munteanu, *Solid State Commun.* **43**, 519 (1982).  
<sup>7</sup>A. Petrou, M. C. Smith, C. H. Perry, J. M. Worlock, and R. L. Aggerwal, *Solid State Commun.* **52**, 93 (1984).  
<sup>8</sup>A. A. Reeder, B. D. McCombe, F. A. Chambers, and G. P. Devane, *Phys. Rev. B* **38**, 4318 (1988).  
<sup>9</sup>P. O. Holtz, M. Sundaram, J. L. Merz, and A. C. Gossard, in *Shallow Impurities in Semiconductors 1988*, edited by B. Monemar (IOP, Bristol, 1989), pp. 27–32.  
<sup>10</sup>D. Gammon, R. Merlin, W. T. Masselink, and H. Morkoç, *Phys. Rev. B* **33**, 2919 (1986).  
<sup>11</sup>E. Glaser, D. Gammon, and B. V. Shanabrook, in *Proceedings of the 12th International Conference on Infrared and Millimeter Waves*, edited by R. J. Temkin (IEEE, New York, 1987), pp. 264a–b.  
<sup>12</sup>X. Liu, A. Petrou, A. L. Moretti, F. A. Chambers, and G. P. Devane, *Superlatt. Microstruct.* **4**, 141 (1988).  
<sup>13</sup>R. Dingle, in *Festkörperprobleme, Advances in Solid State Physics*, edited by H. J. Queisser (Pergamon-Vieweg, Braunschweig, 1975), Vol. 15, pp. 21–48.  
<sup>14</sup>S. R. White and L. J. Sham, *Phys. Rev. Lett.* **47**, 879 (1981).  
<sup>15</sup>G. Bastard, *Phys. Rev. B* **24**, 5693 (1981); **25**, 7484 (1982).  
<sup>16</sup>G. D. Sanders and Y.-C. Chang, *Phys. Rev. B* **31**, 6892 (1985).  
<sup>17</sup>M. Altarelli, U. Ekenberg, and A. Fasolino, *Phys. Rev. B* **32**, 5138 (1985).  
<sup>18</sup>L. C. Andreani, A. Pasquarello, and F. Bassani, *Phys. Rev. B* **36**, 5887 (1987).  
<sup>19</sup>K. S. Chan, *J. Phys. C* **19**, L125 (1986).  
<sup>20</sup>U. Ekenberg and M. Altarelli, *Phys. Rev. B* **35**, 7585 (1987).  
<sup>21</sup>Bangfen Zhu and Kun Huang, *Phys. Rev. B* **36**, 8102 (1987);

Bangfen Zhu, *ibid.* **37**, 4689 (1988).

- <sup>22</sup>L. C. Andreani and A. Pasquarello, *Europhys. Lett.* **6**, 259 (1988).  
<sup>23</sup>G. E. W. Bauer and Tsuneya Ando, *Phys. Rev. B* **38**, 6015 (1988).  
<sup>24</sup>W. Kohn, in *Solid State Physics*, edited by F. Seitz and D. Turnbull (Academic, New York, 1957), Vol. 5.  
<sup>25</sup>F. Bassani, G. Iadonisi, and B. Preziosi, *Rep. Prog. Phys.* **37**, 1099 (1974).  
<sup>26</sup>A. Baldereschi and N. O. Lipari, *Phys. Rev. B* **8**, 2697 (1973).  
<sup>27</sup>G. Bastard, *Phys. Rev. B* **24**, 4714 (1981).  
<sup>28</sup>C. Mailhot, Y.-C. Chang, and T. C. McGill, *Phys. Rev. B* **26**, 4449 (1982).  
<sup>29</sup>R. L. Greene and K. K. Bajaj, *Solid State Commun.* **53**, 1103 (1985).  
<sup>30</sup>F. Bassani, S. Fraizzoli, and R. Buczko, in Ref. 9, pp. 51–56.  
<sup>31</sup>W. T. Masselink, Y.-C. Chang, and H. Morkoç, *Phys. Rev. B* **28**, 7373 (1983); **32**, 5190 (1985); W. T. Masselink, Y.-C. Chang, and H. Morkoç, *J. Vac. Sci. Technol. B* **2**, 376 (1984).  
<sup>32</sup>J. M. Luttinger and W. Kohn, *Phys. Rev.* **97**, 869 (1955).  
<sup>33</sup>J. M. Luttinger, *Phys. Rev.* **102**, 1030 (1956).  
<sup>34</sup>G. Dresselhaus, *Phys. Rev.* **100**, 580 (1955); E. O. Kane, *J. Phys. Chem. Solids* **1**, 249 (1957).  
<sup>35</sup>G. F. Koster, J. O. Dimmock, R. G. Wheeler, and H. Statz, *Properties of the Thirty-Two Point Groups* (MIT Press, Cambridge, MA 1969).  
<sup>36</sup>I. S. Gradshteyn and I. M. Ryzhik, *Table of Integrals, Series and Products*, edited by A. Jeffrey (Academic, New York, 1980).  
<sup>37</sup>*Landolt-Börnstein, Numerical Data and Functional Relationships in Science and Technology*, edited by O. Madelung (Springer, Berlin, 1982), Gp. III, Vol. 17.  
<sup>38</sup>H. C. Casey and M. B. Panish, *Heterostructure Lasers* (Academic, New York, 1978).  
<sup>39</sup>L. E. Oliveira and L. M. Falicov, *Phys. Rev. B* **34**, 8676 (1986).  
<sup>40</sup>A careful analysis of this effect is given by S. Fraizzoli, F. Bassani, and R. Buczko (unpublished).  
<sup>41</sup>R. Buczko, *Nuovo Cimento B* **9**, 669 (1987).  
<sup>42</sup>S. Rodriguez, P. Fisher, and F. Barra, *Phys. Rev. B* **5**, 2219 (1972).  
<sup>43</sup>P. Janiszewski and M. Suffczyński, *Solid State Commun.* **37**, 819 (1981).  
<sup>44</sup>R. F. Kirkman, R. A. Stradling, and P. J. Lin-Chung, *J. Phys. C* **11**, 419 (1978).